Combined experimental and theoretical study on photoionization cross-sections of benzonitrile and o/m/p-cyanotoluene

Jiabin Huang[a], Can Huang[b], Xiaoqing Wu[a,c], Qifeng Hou[a], Guangjun Tian[d], Jiuzhong Yang[c,*], and Feng Zhang[a,*]

[a] *Hefei National Laboratory for Physical Sciences at the Microscale, University of Science and Technology of China, Hefei, Anhui, 230026, P. R. China*

[b] *Chair of Technical Thermodynamics, RWTH Aachen University, 52062 Aachen, Germany*

[c] *National Synchrotron Radiation Laboratory, University of Science and Technology of China, Hefei, Anhui, 230029, P. R. China*

[d] *Key Laboratory for Microstructural Material Physics of Hebei Province, School of Science, Yanshan University, Qinhuangdao 066004, P. R. China*

Abstract

The photoionization cross-sections (PICS) for the products of the reaction from CN with toluene, including benzonitrile and o/m/p-cyanotoluene, were obtained at the photon energies ranging from ionization thresholds to 14 eV by tunable synchrotron vacuum ultraviolet photoionization mass spectrometry (SVUV-PIMS). Theoretical calculations based on the frozen-core Hartree–Fock approximation and Franck-Condon simulations were carried out to cross-verify the measured PICS. The results show that the photoionization cross-sections of benzonitrile and cyanotoluene isomers are similar. The generalized charge decomposition analysis was used to investigate the components of the highest occupied molecular orbital

* Authors to whom correspondence: jzhyang@ustc.edu.cn for JY and feng2011@ustc.edu.cn for FZ

(HOMO) and HOMO-1. It was found that the HOMO and HOMO-1 of benzonitrile and cyanotoluene isomers are dominated by the features of the benzene ring, indicating that the substitution of CN and methyl have a minor influence on the PICS of the studied molecules. The reported PICS on benzonitrile and cyanotoluene isomers in the present work could contribute to the near-threshold PIMS experiments and determine the ionization and dissociation rates in interstellar space for these crucial species. The theoretical analysis on characteristics of molecular orbitals provides clues on estimating PICS of similar substituted aromatic compounds.

I. INTRODUCTION

Toluene has been suggested as an important aromatic compound in the atmosphere of Titan.[1-3] The reaction of toluene with cyano radical (CN) is a crucial channel to incorporate nitrogen into Titan's molecular weight growth model,[4] which ultimately leads to the brown appearance of Titan's atmosphere.[5-7] Previous studies have shown very fast rate coefficients between CN and unsaturated compounds including aromatics at low temperatures.[8, 9] Recently, Messinger et al.[10] investigated this reaction by the pulsed laser photolysis–laser-induced fluorescence (PLP-LIF) technique and quantum chemical calculations, indicating that the rate constants of CN + toluene between 15 and 294 K are independent of temperature, with an average value of $(4.1 \pm 0.2) \times 10^{-10}$ cm^3 $molecule^{-1}$ s^{-1}, at the total gas density from 2.7 to 10.5×10^{16} cm^{-3}. Trevitt et al.[11] have measured the rate coefficients of toluene + CN to be 1.3×10-10 cm^3 $molecule^{-1}$ s^{-1} using a pulsed Laval nozzle expansion in conjunction with laser-induced fluorescence (LIF) at 105 K and 4 Torr. In addition, the reaction products of CN with toluene were detected by using tunable synchrotron VUV photoionization mass spectrometry. The experimental results also revealed

that the main product of the reaction is cyanotoluene. Scheme 1 illustrates four possible reaction products of toluene + CN. CN adds to the benzene ring then removes a hydrogen atom to generate ortho, meta, or para-substituted products. It may also substitute the methyl group to generate benzonitrile.[12-14] In recent years, benzonitrile, as one of the simplest aromatic derivatives, has detected in the cold-core Taurus Molecular Cloud 1 (TMC-1). It provides an important reference for the formation mechanism of PAHs (polycyclic aromatic hydrocarbons) in the ISM (interstellar medium).[15,16] No evidence of benzonitrile formation was observed in the study of Trevitt et al. The lack of photoionization cross-sections (PICS) of various cyanotoluene isomers has hindered the identification of isomers in the SVUV-PIMS experiment.[11]

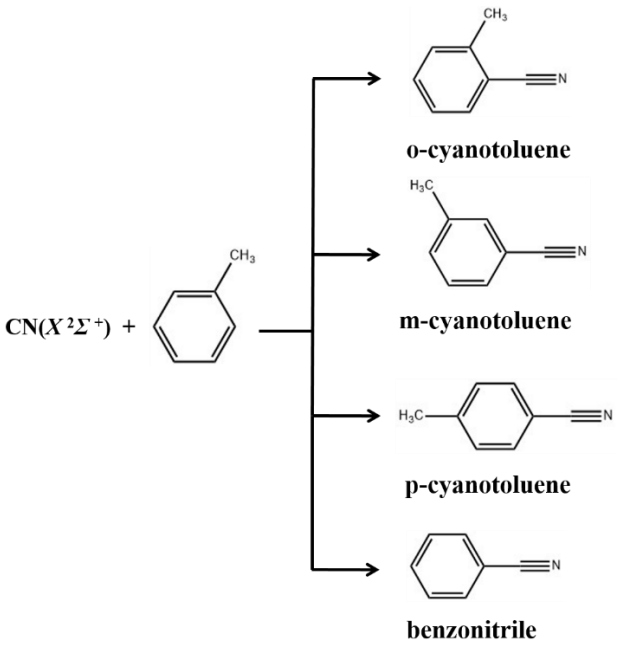

Scheme 1 Main products of CN + Toluene

PICS is the key to quantify the concentration of intermediates in photoionization mass spectrometry experiments,[17-20] which has attracted great attention in the gas phase chemistry communities including atmosphere, interstellar and combustion, etc.[17, 21-23] It is also necessary to determine the ionization and dissociation rates of astrochemical interest in

the field of radiation.[23, 24] Adam et al.[25] measured a series of aromatic hydrocarbons at 10.5 eV for quantitative analysis of complex organic mixtures. Zhou et al.[26] determined the absolute photoionization cross-sections of some aromatics and aromatic derivatives, helping quantitative analysis of combustion intermediates. Recently, Jin et al.[27] added the photoionization cross-sections of 12 aromatic hydrocarbons using tunable SVUV-PIMS. Comparing with the abundant data reported for aromatic hydrocarbons, the photoionization cross-sections of nitrogen-containing aromatic compounds are very scarce.

Theory analysis of the photoionization phenomenon based on the electronic structure calculations has provided a powerful tool for obtaining the photoionization cross-sections. Krylov et al.[28] obtained the Dyson orbital by the EOM-CCSD wave function and calculated the photoionization cross-sections by photoelectron matrix. The theoretical photoionization cross-sections were obtained by using coulomb wave to describe the emitted photoelectron, the results of some atoms and small molecules are in good agreement with the experimental values under the selection of appropriate effective charge. Lucchese et al. [29, 30] has computed PICS of CF_4,[31] SF_6,[32] and N_2[29] using the single-channel frozen-core Hartree-Fock (FCHF) assumption. Kai et al.[33] improved the description of near-threshold photoionization based on of FCHF by multiplying the Franck-Condon overlap envelope with the transition moments. The discrepancy of the computed PICS for a dozen of testing molecules was estimated as less than a factor of 2.[28, 33]

In this present study, the SVUV-PIMS was used to measure the PICS of benzonitrile and o/m/p-cyanotoluene from threshold to 14 eV. Ionization energies of the species have been obtained by state-of-the-art theoretical methods as well. The FCHF method was used to simulate the

photoionization cross-sections. Our goal is not only to provide necessary data for distinguishing product yields of the reaction of toluene + CN, but also to shed light on the PICS of CN substituted aromatics. The CN group has been regarded as an indicator for observing aromatic compounds in the interstellar medium due to the large dipole moments resulted from the CN substituents.[10, 34]

II. EXPERIMENTAL METHODS

Experimental work was carried out in a flow reactor at an undulator-based vacuum ultraviolet (VUV) beamline (BL03U) of the Hefei Light Source at the National Synchrotron Radiation Laboratory (NSRL) in Hefei, China. The apparatus used for this work has been described in previous publications.[21, 35] The samples were vaporized into the 10-mm-diameter flow reactor at 220 - 250 ℃ to ensure full vaporization, the pressure difference between the flow reactor (266 Pa) and differential chamber (0.05 Pa) was large enough so that a molecular beam formed at the quartz nozzle. In the direction of beam propagation, the random directional motion of gas molecules is collimated by a nickel predator, and the acute angle of the sampling cone prevents the backscattered gas from entering the orifice, thus only the sample is emitted directly from the reactor and is extracted. The sample is finally ionized by an orthogonal tunable VUV light beam in the ionization chamber. With the 200 lines mm^{-1} grating, the photon flux of the beamline is higher than 1×10^{13} photons s^{-1} in the energy range of 5 to 25 eV with the full width at half-maximum (FWHM) of 1.87 meV at 7.3 eV (where energy resolution is 3900 at about 7.3 eV).[35]

The ion signal S_i of species i under photon energy E can be written as

$$S_i(T) = C \times X_i \times D_i \times \sigma_i(E) \times \varphi(E) \quad (1)$$

where C is an empirical instrument parameter, which depends on the state of the instrument and the temperature and pressure of the experiment, the

parameter can be considered to be constant in the same experiment. X_i and D_i are the mole fraction and the mass discrimination factor for species i, respectively, σ_i is the photoionization cross-sections of target species at photon energy E, and the $\varphi(E)$ is the photon flux. By taking nitric oxide as the reference species, the expression for converting the signal into the photoionization cross-sections is as:

$$\boldsymbol{\sigma_i} = \boldsymbol{\sigma_{ref}} \times \frac{\boldsymbol{S_i(E)}}{\boldsymbol{S_{ref}(E)}} \times \frac{\boldsymbol{X_{ref}(E)}}{\boldsymbol{X_i(E)}} \times \frac{\boldsymbol{D_{ref}}}{\boldsymbol{D_i}} \tag{2}$$

$$\frac{\Delta\boldsymbol{\sigma_i}}{\boldsymbol{\sigma_i}} = \frac{\Delta\boldsymbol{S_i(E)}}{\boldsymbol{S_i(E)}} + \frac{\Delta\boldsymbol{X_i(E)}}{\boldsymbol{X_i(E)}} + \frac{\Delta\boldsymbol{(D_i)}}{\boldsymbol{D_i}} \tag{3}$$

The error of photoionization cross-section of target species mainly comes from the error caused by D_i, S_i, and X_i, for which the error of D_i is about 20%, the error of Si is about 2% under the current signal-to-noise ratio, and the error caused by X_i can be ignored under the action of the flow controller. According to the relative error transfer formula, the photoionization cross-sections measured in the experiment are expected to have an error of $\pm$20%.

Table 1 Studied molecules and experimental parameters used in this work

Target molecule	Mole fraction	Flowrate	Boil point (°C)	T_{vap} (°C)
benzonitrile	1‰	2.279	190.95	220
o-cyanotoluene	1‰	2.625	205.05	240
m-cyanotoluene	1‰	2.533	214.15	250
p-cyanotoluene	1‰	2.665	217.65	250

Flowrate: liquid injecting flow rate, in μL/min;

T_{vap}: heating temperature of vaporizer;

The studied molecules and experimental parameters used in this work are shown in Table 1, all the target molecules in this work have sufficient

saturated vapor pressure, so they do not need to be dissolved in other reagents. The total flow rate in the flow reactor was 500 SCCM (standard cubic centimeter per minute), the concentration of the tested species-benzonitrile (MACKLIN,99%), o-cyanotoluene (MACKLIN,98%), m-cyanotoluene (MACKLIN,99%), and p-cyanotoluene (MACKLIN,99%)-was 1‰, the concentration of NO as the reference species was 4%, the experiment was carried out under the pressure of 4 Torr and the rest was argon. All chemicals were used without further purification.

III. THEORETICAL METHODS

3.1 Cross-sections

The double hybrid B2PLYP−D3 functional[36] with the Dunning's correlation consistent basis set (triple zeta), i.e. cc-pVTZ, was used to obtain the equilibrium geometries, frequencies, and zero point energies (ZPE) of the neutral molecules and corresponding cations of benzonitrile and o/m/p-cyanotoluene. Single point energies (SPE) were computed at the level of CCSD(T)/aug-cc-pVTZ.[37] The scale factor of 0.983[38] for ZPE correction is adopted.

The cross section is calculated as:

$$\sigma(E) = F(E) \times T(E) \tag{4}$$

The cross-section is the product of the Franck-Condon overlap envelope ($F(E)$) and the transition moments($T(E)$).[33] The Franck-Condon envelope was obtained by the summation and normalization of the Franck-Condon factors computed by the Linear Coupling Model (LCM).[39] The Lorentzian function was used for the line shape broadening of the calculated Franck-Condon transitions. The transition moments were computed within the frozen-core Hartree-Fock approximation,[31, 32] by solving the static-exchange continuum equations with the single-center expansion technique.

L_{max}=50 is used to describe wave functions and E_{max} is set as 50 to specify the maximum value of the electron kinetic energy. The value of *T(E)* in Equation (4) is the average value of the length gauge and the velocity gauge.

In the present work, we considered the contribution of the deep photoionization (photoionization of HOMO-1, HOMO-2, etc.) to better fit the experimental value, where the information of deep ionization energy was referred from the photoelectron spectroscopy as reported in the literature. [40] Based on the deep ionization energy, the total photoionization cross-section is obtained by adding the photoionization cross-sections under each ionization channel, expanding single-channel to multi-channel. It should be noted that because of the indistinguishability of electrons and the Pauli principle, orbitals are not unique and unobservable.[41, 42] It means that it is not rigorous to regard photoelectrons as being in a specific orbital before it is ionized.[43] For the description of photoelectron behavior in photoionization, Dyson orbital is instead a more reasonable way. The Dyson orbital represents the difference between the electron-density distributions of the neutral molecule and its cation.[28, 44, 45] Nevertheless, the concept of the molecular orbital is helpful for the analysis of some experimental phenomena.

All DFT calculations were performed using the Gaussian 16 program, [46] and the CCSD(T) calculations were performed by the ORCA program package.[47] The Franck-Condon factors and transition moments were obtained by the Dynavib[48] and ePolyScat[31, 32] program package, respectively.

3.2 Orbital interaction analysis

To investigate the effect of molecular fragments on the orbitals of the parent molecule, we use the generalized charge decomposition analysis (GCDA) method to do orbital interaction analysis. Dapprichh and Frenking[49] proposed the theory of charge decomposition analysis (CDA).

The electron density function is expressed by Equation (5), where μ, ν represents the fragment orbitals of A and B fragment, m_i represents the occupation numbers, $C_{\mu i}$ and $C_{\nu i}$ represents the expansion coefficient of μ_{th} and ν_{th} fragment orbitals in i_{th} orbital of the parent molecule, and $S_{\mu\nu}$ represents the overlap integral between μ_{th} and ν_{th} fragment orbital.

$$\rho(r) = \sum_i \sum_\mu \sum_\nu m_i C_{\mu i} C_{\nu i} S_{\mu\nu} \tag{5}$$

$$n_i = \sum_\mu \sum_\nu m_i C_{\mu i} C_{\nu i} S_{\mu\nu} \tag{6}$$

The orbital of the parent molecule is described by the basic functions of the atomic center defined by the basis set. The basic functions of the fragment is used to expand the orbital of the parent molecule. Since the number of basic function remains the same, there will be no loss of information in this way. The resulting expansion coefficient can be used to obtain the composition values of the fragment orbital corresponding to the parent molecule orbital. Xiao and Lu[50] proposed the generalized CDA (GCDA) method. GCDA deals with alpha and beta electron separately which solves the problem that CDA can only be used in closed-shell systems. In this work, we use the expansion coefficient to draw the orbital interaction diagram to investigate the main components of parent molecule orbitals. The generalized orbital interaction analysis was performed by the Multiwfn program.[51]

IV. RESULTS AND DISCUSSION

4.1 Absolute cross-sections

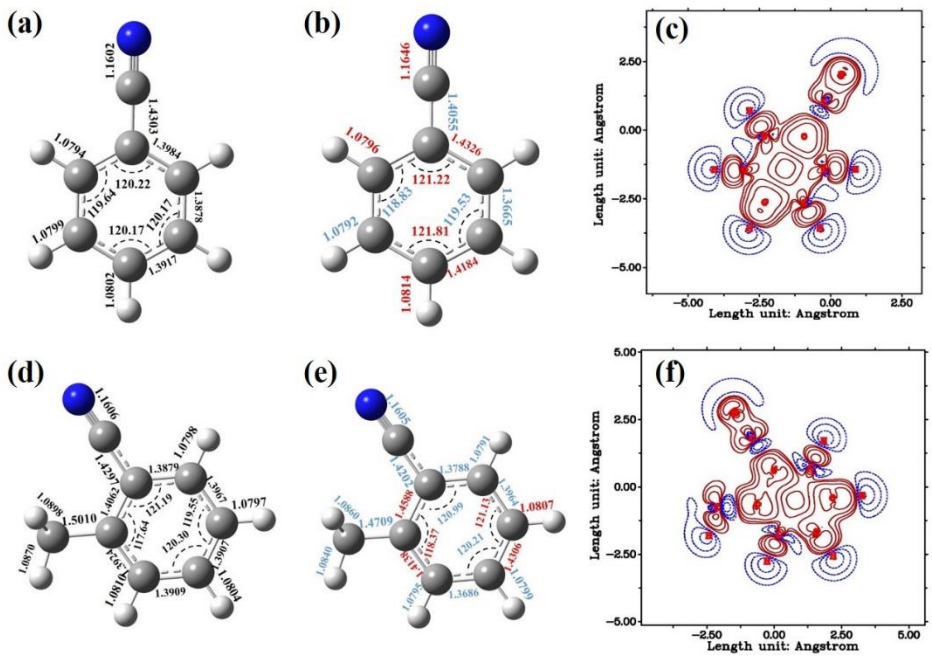

Figure 1 The change of the geometric structure of benzonitrile and o-cyanotoluene after ionization, (a) and (b) correspond to the geometric structure of the neutral and ionic ground state benzonitrile, (d) and (e) correspond to the geometric structure of neutral and ionic ground state of o-cyanotoluene, the red number indicates the bondd length/angles increased after ionization, and blue represents the decreased ones (Å). (c) and (f) are the electron density maps of the difference between molecules and corresponding cations on the X-Y plane of the benzonitrile and o–cyanotoluene, The red shows the contours with increased electron density, and the blue shows the contours with decreased electron density.

Figure 1 shows the ground state structure of the neutral and cations of benzonitrile and o-cyanotoluene. The change of electron density in the process of ionization leads to the geometric difference between neutral molecules and ions. The decrease of electron density will weaken the carbon-carbon bond, consequently elongate the C-C bond length or enlarge the bond angle (shown in red numbers), the increase of electron density will strengthen the carbon-carbon bond and shorten the bond length (blue number). CN is a typical electrophilic group, which is an meta directors and guides other substituents to meta-position. On the contrary, CH_3 is a nucleophilic group and ortho/para-director, which leads the substituent group to ortho-position and para-position. This conflicting effect weakens the C-C bond of CN and CH_3 to benzene ring in varying degrees. The electron absorption ability of CN is stronger than that of CH_3, so the

weakening of C-C bond on CH_3 is more obvious. According to the electron density maps of the difference between molecules and corresponding cations, the electron loss mainly occurs above the plane of the benzene ring (π electron), and the acquisition of electrons occurs inside the plane during ionization. The change of geometry and electron density after ionization of meta and para is similar to that of ortho, as shown in Figure S1 of the supplement. The isosurface of electron density before and after ionization of benzonitrile and o/m/p-cyanotoluene were shown in Figure S2. There is negligible deformation in the geometric structure of cyanotoluene after photoionization, the original symmetry of the system is not broken. As a result, the maximum of Franck-Condon factor appears near the threshold ionization energy, then it decreases with the photon energy (Figure S3-S4 in the supplementary materials).

Table 2 Absolute ionization energies (AIE) and vertical ionization energies (VIE) of benzonitrile and o/m/p-cyanotoluene obtained in this work and from previous literature (Unit: eV)

Species	AIE		Experimental values in the literature	VIE
	Theory	EXP		Theory
benzonitrile	9.71	$9.70^{+0.01}_{-0.01}$	9.71[52];9.73[53]	9.82
o-cyanotoluene	9.39	$9.37^{+0.01}_{-0.01}$	9.40[40];9.38[54];9.39[55]	9.48
m-cyanotoluene	9.40	$9.39^{+0.01}_{-0.01}$	9.34[40];9.30[54];9.40[55]	9.50
p-cyanotoluene	9.31	$9.29^{+0.01}_{-0.01}$	9.38[40];9.33[54];9.32[55]	9.46

Table 2 lists our calculated and experimental adiabatic ionization energies (AIEs) of benzonitrile and o/m/p-cyanotoluene comparing with previous studies. Our calculations are in good agreement with the experimental results with deviations less than 0.03 eV. The largest discrepancy between this work and literature is less than 0.1 eV. The relative

energy difference between the isomers in Table S1 shows that the o-cyanotoluene molecule presents as the most stable isomer among the three cyanotoluenes, while the m-cyanotoluene cation has the lowest energy after ionization. As a result, the AIE of ortho-isomer is similar to that of meta-isomer. Also, due to the substitution of the electron donating group (methyl), the electron density of the benzene ring increases, which reduces the ionization energy of cyanotoluene relative to benzonitrile. The computed vertical ionization energie (VIE) of the four species are also shown in Table 2.

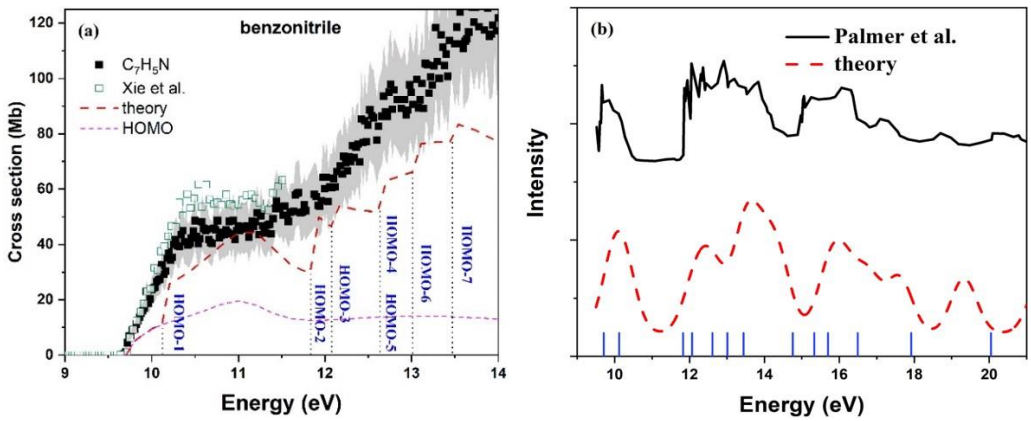

Figure 2 Photoionization cross-sections (a) and photoelectron spectrum (b) from experiment together with theory values of benzonitrile. The green open squares are measurements of Xie et al. (Ref.53). Shadows in (a) represent the error of our experimental measurements. The red dash line in (a) is the result of the Eq. 4, the pink dash indicates the contribution of HOMO. The black solid line in (b) was experimental results adopted from Palmer et al. (Ref.38), the red dash line is our simulated photoelectron spectrum. The black vertical dashed lines in (a) and blue lines in (b) are the ionization energy of different orbitals.

The measured photoionization cross-sections of benzonitrile is shown in Figure 2(a) by black square symbols. Our measurements are lower than those of Xie et al.,[53] which is due to the smaller mass discrimination factor used here. The mass discrimination factor of 0.55 was derived by Jin et al. fitting their new experiments on some aromatic hydrocarbons.[27] The photoionization cross-sections rises smoothly in the FC region since the geometric configuration of the ionization state and the neutral state does

not appear to obviously change. The Franck-Condon envelope converges at about 0.5 eV higher than the threshold energy (9.70 eV), then the cross-sections keeps as ~42 Mb until the photon energy achieves 11.5 eV. It indicates no obvious influence of the excited state in the platform region. The red dash and blue dotted lines shown in Figure 2(a) are our simulations by the single-channel FCHF (only considering the contribution of HOMO) and multi-channel FCHF (including contributions from HOMO-1 to HOMO-7) approximations, respectively. The ionization energy of deep orbitals was taken from the photoelectron spectrum measured by Palmer et al.[40] We also simulated the photoelectron spectrum shown in Figure 2(b) at the level of B2PLYP-D3/cc-pVTZ, which well reproduces the experiments. The straight line represents the ionization energy required to ionize electrons from different orbitals. Figure 2 demonstrates great contribution from deep orbitals. The photoionization from the HOMO accounts for only about half of the near-threshold photoionization cross-sections, which can be explained by the near degenerate HOMO and HOMO-1 in benzonitrile. No further deep ionization occurs in the energy range of 10.5 eV to 12 eV leading to the platform region. With increasing photon energy, more deep orbitals (HOMO-2 to HOMO-7) are involved in the photoionization process.

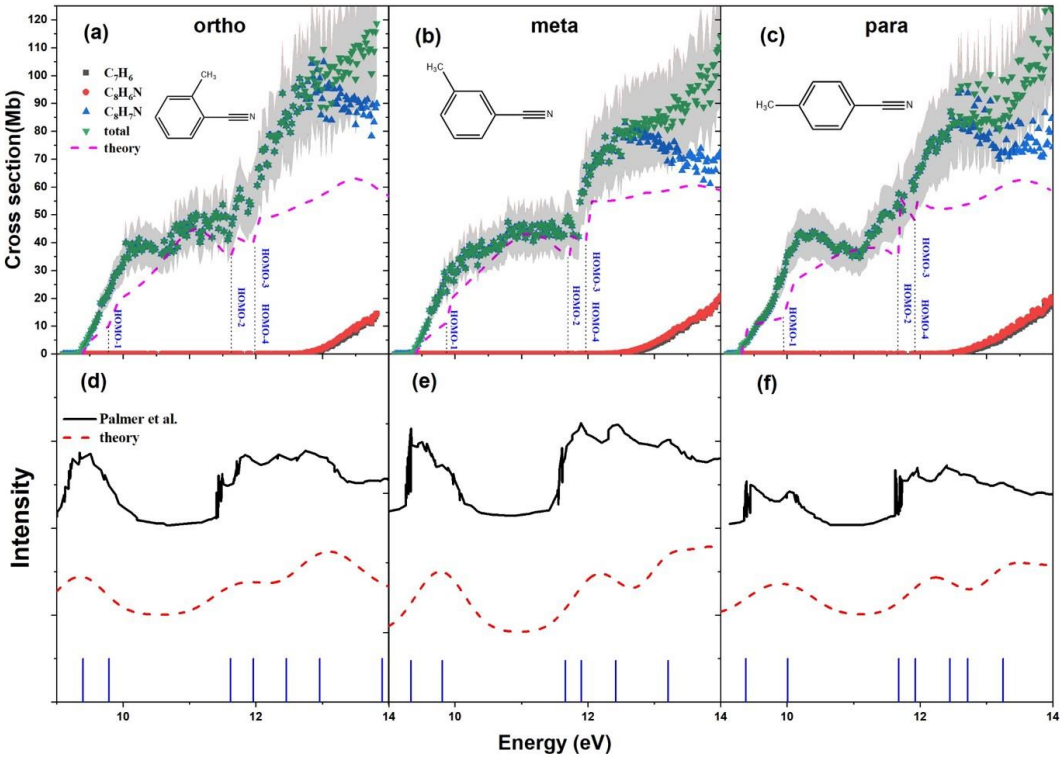

Figure 3 Photoionization cross-sections and photoelectron spectrum from experiments together with theoretical predictions of o-cyantoluene (a) (d), m-cyanotoluene (b) (e), p-cyanotoluene (c) (f). The pink dash line in (a-c) is the result of the Eq. 4. The black solid line in (d-f) was experimental results adopted from Palmer et al. (Ref.38), the red dash line is our simulated photoelectron spectrum. The black vertical dashed lines in (a-c) and blue lines in (d-f) are the ionization energy of different orbitals.

Figure 3 shows the measured and calculated photoionization cross-sections of o/m/p-cyanotoluene. In the supplement, we provide enlarged cross sections at about 2.5 eV after the threshold to give more detailed features (see Figure S5). Similar to that of benzonitrile, the FC region involves the contribution from the HOMO-1 orbital for each cyanotoluene isomer. A plateau region exists about 1.5 eV behind the FC region, and then the cross-sections continues to increase. When the photon energy rises to about 3 eV higher than the threshold, the cyanotoluene cations tend to dissociate. Considering the dissociation dynamics at high energies, we only include the contribution of deep orbitals with ionization energies lower than the dissociation energy, i.e. HOMO-1 to HOMO-4 for o- and m-

cyanotoluene, HOMO-1 to HOMO-3 for the para-isomer. The fragments signal of C_7H_6 and C_8H_6N are also shown in Figure 3. The o-cyanotoluene and p-cyanotoluene show characteristics similar to shape resonance at about 12.3 eV. The shape resonance is caused by the temporary trapping of photoelectrons with high angular momentum by the centrifugal barrier in the electron−ion potential, the shape resonance has a great influence on the cross-sections, final state branching ratio, and photoelectron angular distribution.[56,57] Due to the high *l* characteristic of virtual orbitals, the photoionization absorption cross-sections of linear internal alkynes show obvious shape resonance characteristics.[56,58] The shape resonance characteristics near the threshold photoionization of p-cyanotoluene indicates a similar effect of the carbon-nitrogen triple bond as the carbon-carbon triple bond. The related mechanism needs to be further studied. In the multi-channel FCHF, we only simulate the process of direct ionization without considering the effects of autoionization and shape resonance. The theoretical simulation indicates a broad peak in simulation at ~11 eV. The pick comes from the contribution of the scattering of electrons from the irreducible A_1 state (initial state) to the total final state (target state and the continuum electron) whose the symmetry is A_1. The large transition moment of these two states makes the simulation value mainly reflects the characteristics of this channel.

4.2 Orbital interaction analysis

The measured absolute values of PICS for benzonitrile and three cyanotoluene isomers are quite close over the studied energy range. To further reveal the relationship between photoionization cross-sections and molecular structures, we use the GCDA method[50] to explore the influence of substituent positions on valence orbitals involved in the threshold photoionization process. The details of this analysis method have been

given in section 3.2.

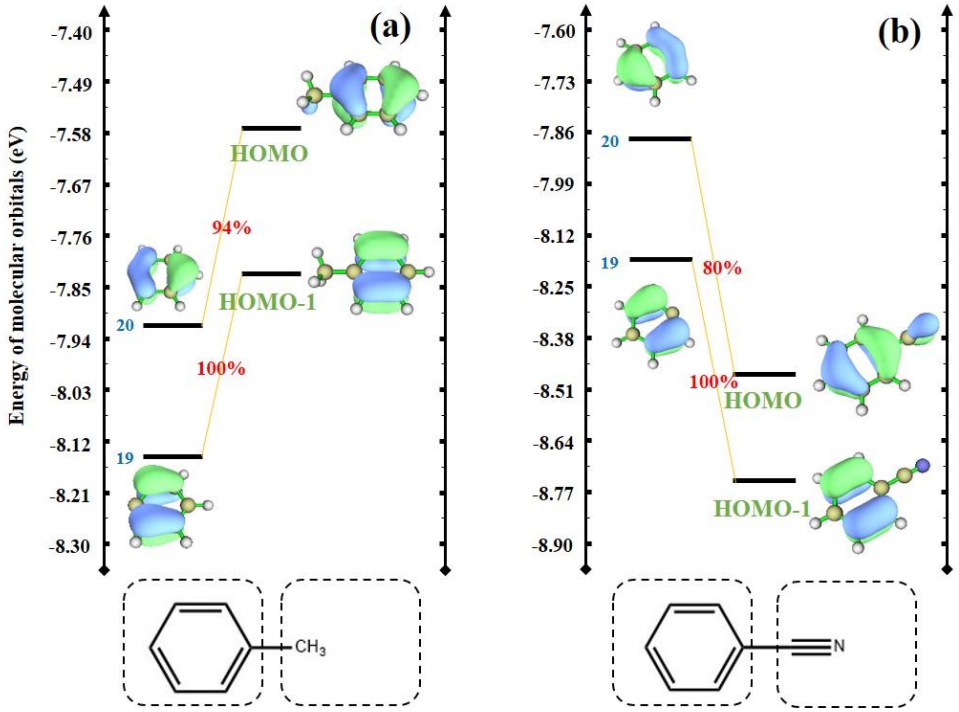

Figure 4 The orbital interaction diagram of (a) toluene and (b) benzonitrile, split toluene into phenyl and methyl, split benzonitrile into phenyl and CN, the black horizontal line represents the molecular orbital, the blue number represents the molecular orbital number of phenyl, and the red number represents the component of the fragment orbital in the molecular orbital of the complex the corresponding molecular orbitals are given.

For benzonitrile and cyanotoluene isomers, the near-threshold photoionization corresponds to the photoionization of electrons on HOMO and HOMO-1. Figure 4 (a) and (b) show the orbital interaction diagrams of HOMO and HOMO-1 of toluene and benzonitrile respectively. The fragment orbitals are calculated separately maintaining the same geometric structure as in the corresponding molecule. Tklhe longitudinal coordinate represents the orbital energy. Those red numbers display the composition of the fragment orbitals in the parent molecule orbitals. Figure 4 demonstrates that the delocalized π electrons on the benzene ring make dominant contributions to the HOMO and HOMO-1 of benzonitrile and toluene. The shapes of HOMO and HOMO-1 of toluene and benzonitrile are basically

consistent with the corresponding HOMO (NO.20) and HOMO-1 (NO.19) of phenyl fragments, which reflects the characteristics of benzene ring. The electron energy of the CH3 and CN fragments is very low compared with the parent molecules, and the contribution to the HOMO and HOMO-1 is negligible, so it is not shown in the energy region of figure 4. The contribution of phenyl to the HOMO of benzonitrile (80%) is slightly lower than that of HOMO in toluene (94%), because CN is an electron-withdrawing group while CH_3 is an electron-donating group.

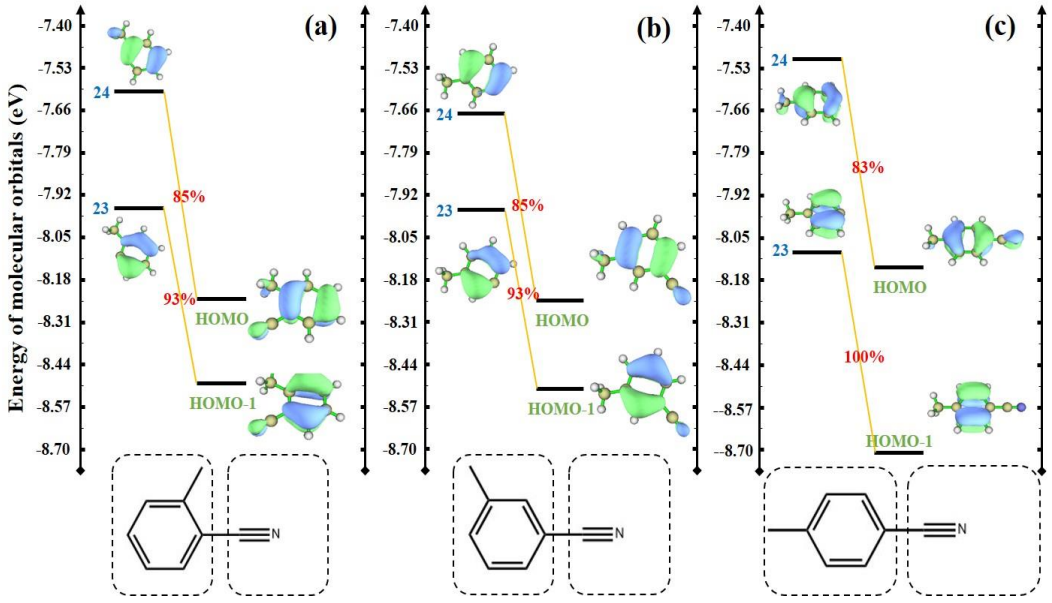

Figure 5 The orbital interaction diagram of (a) o-cyanotoluene, (b) m-cyanotoluene and (c) p-cyanotoluene, splitting cyanotoluene into tolyl and CN. The blue number represents the molecular orbital number and the red number represents the component of the fragment orbital in the molecular orbital of the parent molecule.

Figure 5 shows the orbital interaction diagram of HOMO and HOMO-1 for the o/m/p-cyanotoluene isomers. The HOMO and HOMO-1 of the three cyanotoluene molecules basically reproduce the characteristics of molecular orbitals of the benzene ring (> 80%). In other words, the di-substitution of -CN and -CH_3 does not change the main feature of HOMO and HOMO-1 orbitals, comparing with the mono-substituted benzonitrile and toluene.

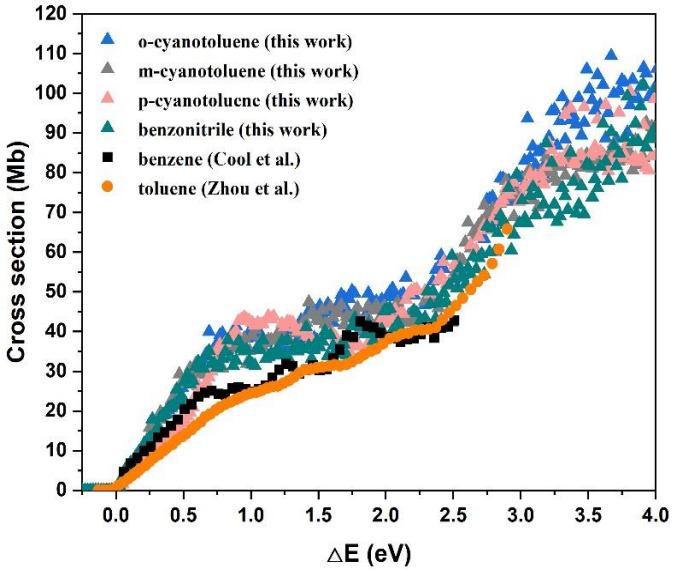

Figure 6 Comparison of the photoionization cross-sections of benzonitrile, o/m/p-cyanotoluene, benzene (Ref.18), and toluene (Ref.24). ΔE is photon energy above the ionization energy.

The GCDA analysis indicates that the electronic configuration of the benzene ring dominates the feature of HOMO and HOMO-1 of toluene, benzonitrile, and o/m/p-cyanotoluene isomers. It explains the similarity of the PICS of these species, as illustrated by Figure 6. The ΔE in the horizontal coordinate is the photon energy relative to the first ionization energy. The PICS of benzonitrile and o/m/p-cyanotoluene isomers show strong similarity with photon energy up to 2.5 eV higher than the threshold. The molecule orbital shape for the HOMO and HOMO-1 of toluene and benzene are basically consistent, so the photoionization cross-sections of toluene[26] and benzene[20] are very similar. Besides, compared with other aromatic compounds, benzene has the highest symmetry, it shows obvious Rydberg states characteristics.[20, 59] It's interesting to see the key role of the benzene ring during photoionization for the studied aromatics. Nevertheless, if this finding can be extrapolated to other mono- or di-aromatic compounds requires further investigation on the effect of various substitutions.

V. CONCLUSION

In this work, the photoionization cross-sections of benzonitrile and o/m/p-cyanotoluene over the photon energy range of threshold to 14 eV, products of the reaction between CN and toluene, were investigated by both experimental measurements and theoretical calculations. The technique of synchrotron vacuum ultraviolet photoionization mass spectrometry was employed. The frozen-core Hartree–Fock approximation was the key approximation for the theoretical prediction. The contribution of the deep orbital photoionization was included to simulate the multi-channel photoionization. It was revealed that the photoionization of HOMO-1is involved in the Franck-Condon region for benzonitrile and cyanotoluene isomers, and deeper orbitals also have contributions with increasing the photon energy by ~2 eV higher than the threshold. To study the effect of CN and methyl substitution on the molecular orbitals of aromatic compounds, we used the generalized charge decomposition analysis method to investigate the composition of the orbitals. It shows that the HOMO and HOMO-1 of benzonitrile and cyanotoluene reflect the characteristics of the benzene ring, i.e., the substitution sites of CN and methyl do not change the dominant position of benzene ring. As a result, photoionization cross-sections of benzonitrile and cyanotoluene isomers are very similar. The reported PICS on benzonitrile and cyanotoluene isomers are valuable for quantifying these key species and calculating related parameters in interstellar space. The findings of dominant contribution from the benzene ring on HOMO and HOMO-1 of the studied molecules have the potential to estimate the near-threshold PICS of other substituted aromatic compounds.

VI. SUPPLEMENTARY MATERIAL

See supplementary material for the electron density maps and calculated Franck-

Condon factors of the benzonitrile and o/m/p-cyanotoluene.

VII. ACKNOWLEDGMENTS

This work was financially supported by the National Natural Science Foundation of China (51876199), the National Key Research and Development Program of China (Grant No. 2016YFC0202600), and the Chinese Universities Scientific Fund (WK2310000069). The quantum chemistry calculations are completed on the Hanhai 20 supercomputing system of the Supercomputing Center of the University of Science and Technology of China. We are grateful to Professor Robert R. Lucchese for kindly providing us the ePolyScat code and many suggestions.

VIII. DATA AVAILABILITY

The data that support the findings of this study are available from the corresponding author upon reasonable request.

IX. REFERENCES

1. J. Cui, R. Yelle, V. Vuitton, J. Waite Jr, W. Kasprzak, D. Gell, H. Niemann, I. Müller-Wodarg, N. Borggren and G. Fletcher, Icarus **200** (2), 581-615 (2009).
2. V. Vuitton, R. Yelle and J. Cui, Journal of Geophysical Research: Planets **113** (E5) (2008).
3. B. A. Magee, J. H. Waite, K. E. Mandt, J. Westlake, J. Bell and D. A. Gell, Planet. Space Sci. **57** (14-15), 1895-1916 (2009).
4. A. J. Trevitt and F. Goulay, Phys. Chem. Chem. Phys. **18** (8), 5867-5882 (2016).
5. C. Sagan, B. Khare, W. Thompson, G. McDonald, M. R. Wing, J. L. Bada, T. Vo-Dinh and E. Arakawa, Astrophys. J. **414**, 399-405 (1993).
6. E. Wilson and S. Atreya, Planet. Space Sci. **51** (14-15), 1017-1033 (2003).
7. M. Delitsky and C. McKay, Icarus **207** (1), 477-484 (2010).
8. K. L. Gannon, D. R. Glowacki, M. A. Blitz, K. J. Hughes, M. J. Pilling and P. W. Seakins, J. Phys. Chem. A **111** (29), 6679-6692 (2007).
9. J. C. Loison, E. Hébrard, M. Dobrijevic, K. M. Hickson, F. Caralp, V. Hue, G. Gronoff, O. Venot and Y. Bénilan, Icarus **247**, 218-247 (2015).
10. J. Messinger, D. Gupta, I. R. Cooke, M. Okumura and I. R. Sims, J. Phys. Chem. A **124** (39), 7950-7958 (2020).

11. A. J. Trevitt, F. Goulay, C. A. Taatjes, D. L. Osborn and S. R. Leone, J. Phys. Chem. A **114** (4), 1749-1755 (2010).
12. N. B. Henis and L. L. Miller, J. Am. Chem. Soc. **105** (9), 2820-2823 (1983).
13. P. Spagnolo, L. Testaferri and M. Tiecco, J. Chem. Soc. B, 2006-2008 (1971).
14. Y. So and L. L. Miller, J. Am. Chem. Soc. **103** (14), 4204-4209 (1981).
15. B. A. McGuire, A. M. Burkhardt, S. Kalenskii, C. N. Shingledecker, A. J. Remijan, E. Herbst and M. C. McCarthy, Science **359** (6372), 202-205 (2018).
16. M. C. McCarthy and B. A. McGuire, The Journal of Physical Chemistry A (2021).
17. O. Kostko, B. Bandyopadhyay and M. Ahmed, Annu. Rev. Phys. Chem. **67**, 19-40 (2016).
18. J. Loison, M. Dobrijevic and K. Hickson, Icarus **329**, 55-71 (2019).
19. J. Wang, B. Yang, T. A. Cool, N. Hansen and T. Kasper, Int. J. Mass spectrom. **269** (3), 210-220 (2008).
20. T. A. Cool, J. Wang, K. Nakajima, C. A. Taatjes and A. Mcllroy, Int. J. Mass spectrom. **247** (1-3), 18-27 (2005).
21. F. Qi, Proc. Combust. Inst. **34** (1), 33-63 (2013).
22. J. M. Dyke, Phys. Chem. Chem. Phys. **21** (18), 9106-9136 (2019).
23. H. R. Hrodmarsson, G. A. Garcia, L. Nahon, J.-C. Loison and B. Gans, Phys. Chem. Chem. Phys. **21** (46), 25907-25915 (2019).
24. A. Heays, A. Bosman, van and E. Van Dishoeck, A&A **602**, A105 (2017).
25. T. Adam and R. Zimmermann, Anal. Bioanal. Chem. **389** (6), 1941-1951 (2007).
26. Z. Zhou, M. Xie, Z. Wang and F. Qi, Rapid Commun. Mass Spectrom. **23** (24), 3994-4002 (2009).
27. H. Jin, J. Yang and A. Farooq, Rapid Commun. Mass Spectrom. **34** (21), e8899 (2020).
28. S. Gozem, A. O. Gunina, T. Ichino, D. L. Osborn, J. F. Stanton and A. I. Krylov, J. Phys. Chem. Lett. **6** (22), 4532-4540 (2015).
29. R. R. Lucchese, G. Raseev and V. McKoy, Phys. Rev. A **25** (5), 2572 (1982).
30. R. R. Lucchese and V. McKoy, J. Phys. Chem. **85** (15), 2166-2169 (1981).
31. F. A. Gianturco, R. R. Lucchese and N. Sanna, J. Chem. Phys. **100** (9), 6464-6471 (1994).
32. A. P. Natalense and R. R. Lucchese, J. Chem. Phys. **111** (12), 5344-5348 (1999).
33. K. Moshammer, A. W. Jasper, D. M. Popolan-Vaida, Z. Wang, V. S. Bhavani Shankar, L. Ruwe, C. A. Taatjes, P. Dagaut and N. Hansen, J. Phys. Chem. A **120** (40), 7890-7901 (2016).
34. E. Herbst and E. F. Van Dishoeck, ARA&A **47**, 427-480 (2009).
35. Z. Zhou, X. Du, J. Yang, Y. Wang, C. Li, S. Wei, L. Du, Y. Li, F. Qi and Q. Wang, Journal of Synchrotron Radiation **23** (4), 1035-1045 (2016).
36. S. Grimme, J. Chem. Phys. **124** (3), 034108 (2006).
37. K. Kowalski and P. Piecuch, J. Chem. Phys. **113** (1), 18-35 (2000).
38. B. Chan and L. Radom, J. Chem. Theory Comput. **12** (8), 3774-3780 (2016).

39. P. Macak, Y. Luo and H. Ågren, Chem. Phys. Lett. **330** (3-4), 447-456 (2000).
40. M. H. Palmer, W. Moyes and M. Spiers, J. Mol. Struct. **62**, 165-187 (1980).
41. E. R. Scerri, J. Chem. Educ. **77** (11), 1492 (2000).
42. P. Mulder, Int. J. Philos. Chem **17** (1), 24-35 (2011).
43. D. G. Truhlar, P. C. Hiberty, S. Shaik, M. S. Gordon and D. Danovich, Angew. Chem. Int. Ed. **58** (36), 12332-12338 (2019).
44. C. Melania Oana and A. I. Krylov, J. Chem. Phys. **127** (23), 234106 (2007).
45. J. V. Ortiz, in *Annu. Rep. Comput. Chem.* (Elsevier, 2017), Vol. 13, pp. 139-182.
46. M. Frisch, G. Trucks, H. Schlegel, G. Scuseria, M. Robb, J. Cheeseman, G. Scalmani, V. Barone, G. Petersson and H. Nakatsuji, (Gaussian, Inc. Wallingford, CT, 2016).
47. F. Neese, Wiley Interdisciplinary Reviews: Computational Molecular Science **8** (1), e1327 (2018).
48. S. D. Guangjun Tian, Weijie Hua, Yi Luo, Royal Institute of Technology: Stockholm (2012).
49. S. Dapprich and G. Frenking, J. Phys. Chem. **99** (23), 9352-9362 (1995).
50. M. Xiao and T. Lu, J. Adv. Phys. Chem **4**, 111-124 (2015).
51. T. Lu and F. Chen, J. Comput. Chem. **33** (5), 580-592 (2012).
52. K. Watanabe, T. Nakayama and J. Mottl, J. Quant. Spectrosc. Radiat. Transfer **2** (4), 369-382 (1962).
53. M. Xie, Z. Zhou, Z. Wang, D. Chen and F. Qi, Int. J. Mass spectrom. **303** (2-3), 137-146 (2011).
54. T. Kobayashi and S. Nagakura, Bull. Chem. Soc. Jpn. **47** (10), 2563-2572 (1974).
55. K. Suzuki, S.-i. Ishiuchi, M. Sakai and M. Fujii, J. Electron. Spectrosc. Relat. Phenom. **142** (3), 215-221 (2005).
56. U. Jacovella, D. M. Holland, S. Boyé-Péronne, B. Gans, N. de Oliveira, K. Ito, D. Joyeux, L. Archer, R. R. Lucchese and H. Xu, J. Phys. Chem. A **119** (50), 12339-12348 (2015).
57. M. Piancastelli, J. Electron. Spectrosc. Relat. Phenom. **100** (1-3), 167-190 (1999).
58. H. Xu, U. Jacovella, B. Ruscic, S. Pratt and R. Lucchese, J. Chem. Phys. **136** (15), 154303 (2012).
59. E. Rennie, C. Johnson, J. Parker, D. Holland, D. Shaw and M. Hayes, Chem. Phys. **229** (1), 107-123 (1998).